ACS OMEGA

http://pubs.acs.org/journal/acsodf

Perspective

Recent Advancements in Nontoxic Halide Perovskites: Beyond Divalent Composition Space

Dhirendra Kumar,[⊥] Jagjit Kaur,[⊥] Prajna Parimita Mohanty, Rajeev Ahuja,* and Sudip Chakraborty*

Cite This: *ACS Omega* 2021, 6, 33240−33252

Read Online

ACCESS | Metrics & More | Article Recommendations

ABSTRACT: Since the inception of organic−inorganic hybrid perovskites of ABX_3 stoichiometry in 2009, there has been enormous progress in envisaging efficient solar cell materials throughout the world, from both the theoretical and experimental perspectives. Despite achieving 25.5% efficiency, hybrid halide perovskites are still facing two main challenges: toxicity due to the presence of lead and device stability. Two particular families with $A_3B_2X_9$ and $A_2MM'X_6$ stoichiometries have emerged to address these two prime concerns, which have restrained the advancement of solar energy harvesting. Several investigations, both experimental and theoretical, are being conducted to explore the holy-grail materials, which could be optimum for not only efficient but also stable and nontoxic photovoltaics technology. However, the trade-off among stability, efficiency, and toxicity in such solar energy materials is yet to be completely resolved, which requires a systematic overview of $A_3B_2X_9$- and $A_2MM'X_6$-based solar cell materials. Therefore, in this timely and relevant perspective, we have focused on these two particular promising families of perovskite materials. We have portrayed a roadmap projecting the recent advancements from both theoretical and experimental perspectives for these two exciting and promising solar energy material families while amalgamating our critical viewpoint with a future outlook.

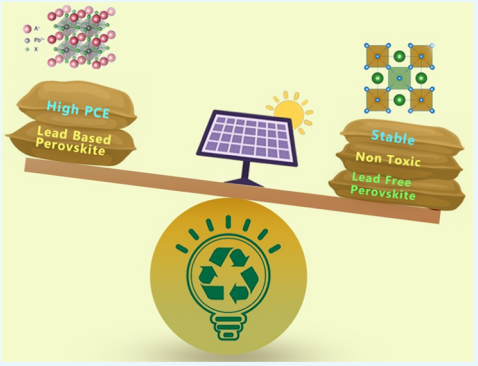

1. INTRODUCTION

The development of a nation implicitly depends on energy production, energy management, and its wise utilization. Most countries nowadays rely on conventional sources of energy, which are going to end very soon and will lead to energy crisis. Energy crisis is a combined effect of overconsumption, overpopulation, poor management, and lack of awareness. Overcoming the energy crisis is the biggest challenge before the scientific community. Focused research on nonconventional, sustainable, and most importantly renewable energy sources is needed to address the current energy scenario. Solar energy is the most promising candidate among all of the emerging renewable energy sources. Solar energy certainly has many advantages over other forms of sustainable sources like easy harvesting, relatively cleaner, low maintenance, and cost-effective. Solar cell technology has significantly evolved over the past few decades, including silicon-based solar cells, Si−Ge thin-film solar cells, dye-sensitized solar cells, and quantum dot sensitized solar cells.[1] Nowadays, perovskite-based solar cells (PSCs) are trending worldwide and inspiring research communities all across the globe. They have appreciable properties like low fabrication cost, high photoconversion efficiency, wide tunable band gap, high absorption coefficient, long charge carrier diffusion length, high charge carrier mobility, high open-circuit voltage, etc.[2] The perovskite structure has the stoichiometry ABX_3, where A is the organic or inorganic ligand, B is the metal cation, and X is the halogen element. Perovskites are highly versatile. They have many optoelectronic applications, namely, photodetectors, X-ray detectors, photocatalysts, light-emitting diodes (LEDs), and solar cells.[3] The power conversion efficiency of perovskite materials increased significantly to 25.5% in 2020.[4,66] In spite of the high conversion efficiency, PSCs have stability issues when exposed to ambient atmospheric conditions. Perovskites have a shorter lifetime as compared to silicon cells because they collapse easily. Instability in the structure arises due to the presence of oxygen and moisture in the atmosphere. Here, the water molecule gets trapped in the perovskite and acts as a catalyst for structure degradation. Perovskites are also highly sensitive to elevated temperatures; as the temperature increases above 100 °C, degradation occurs. A stable perovskite should be able to withstand temperatures above 85 °C.[5] The optoelectronic performance of the device is greatly influenced by other parameters apart from temperature, moisture, and

Received: September 26, 2021
Accepted: November 16, 2021
Published: November 30, 2021

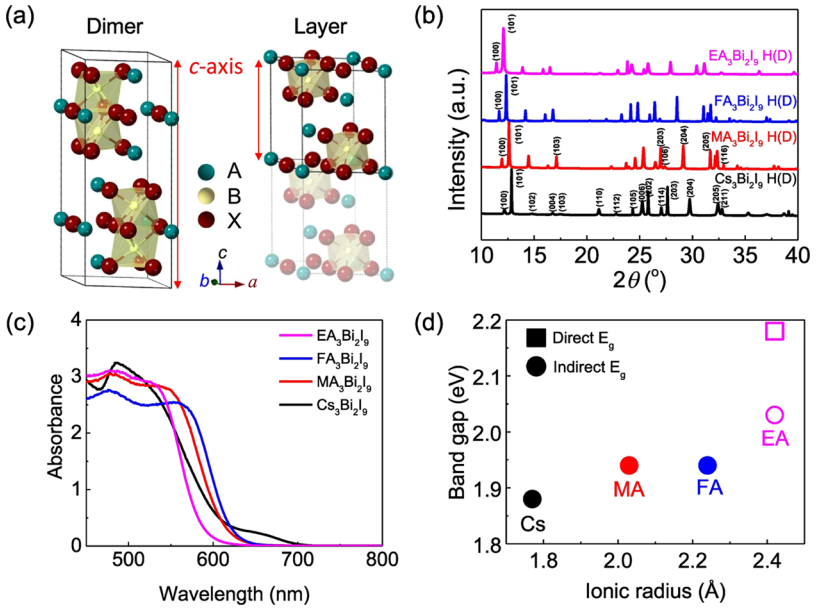

Figure 1. (a) Schematic of the crystal structures of dimer- and layer-type $A_3Bi_2I_9$. (b) X-ray diffraction (XRD) patterns, (c) ultraviolet−visible (UV−vis) absorption spectra, and (d) optical band gap (E_g) of $A_3Bi_2I_9$ (A = Cs, MA, FA, and EA), as a function of A-site ion size. Solid markers in (d) are used if the type of band gap (direct or indirect) is reported, and open markers if not. Reprinted with permission from ref 11. Copyright 2019 Elsevier.

oxygen. PSC technology should address the issues of degradation caused by oxygen, moisture, high temperature, and other environmental factors.

Lead-incorporated organic−inorganic halide perovskites solar cells have already established a theoretical power conversion efficiency of around 31.4%.[6] Consistent use of lead can cause numerous fatal health hazards, which is a threat to society. Hence, toxicity of lead is the largest hurdle to commercialization, which needs to be resolved to give shape to the fantasies over years. Two types of corrective measures can be taken to avoid the discussed concern: (i) replacing lead partially with another less-toxic metal; and (ii) completely replacing lead with like metal elements.[7] Bi and Sb, having a similar electronic configuration as Pb, are answers to the toxicity concern. Advanced research on lead-free perovskites is focusing on different fresh groups of perovskites, namely, trivalent metal-based perovskites ($A_3M_2X_9$; A = Rb/Cs/MA/FA, M = Sb/Bi), tetravalent metal-based perovskites (A_2MX_6; M in the +4 state), and mixed double perovskites ($A_2MM'X_6$; A = Cs/Rb/K, M and M′ in +1 and +3 states, respectively).[8] With a similar electronic configuration and equivalent effective ionic radius, Bi^{3+} and Sb^{3+} are perfect nontoxic alternatives to Pb^{2+}. $A_3M_2X_9$ perovskites can be categorized as Bi-based perovskites and Sb-based perovskites on the basis of M-site metal cation substitution. Sb^{3+} is a stable oxidation state, so Sb-based perovskites have a lower dimensionality like a two-dimensional (2D) layered structure ($P\bar{3}m1$) or a zero-dimensional (0D) dimer structure ($P6_3/mmc$). Sb-based perovskite materials have excellent optoelectronic features and stability. Mixed double perovskites are formed by replacing Pb^{2+} with monovalent and trivalent cations having stoichiometry $A_2M(I)M'(III)X_6$. M^+ sites can be occupied by IA, IB, and IIIA group elements, and M'^{3+} sites can be filled with IIB, IIIA, and VA group elements. $Cs_2AgBiBr_6$ and Cs_2NaBiI_6 are commonly used in photovoltaic applications.[9] $Cs_2AgBiBr_6$ has an indirect band gap of 1.95 eV and possesses excellent stability against moisture and temperature, but starts degrading after a few weeks.

2. LEAD-FREE TRIVALENT HALIDE PEROVSKITES WITH $A_3B_2X_9$ STOICHIOMETRY

In addition to improving the encapsulation of perovskites, another option is to replace Pb with other nontoxic inorganic elements. Beyond group 14 elements, two of group 15 metals in the periodic table, bismuth (Bi) and antimony (Sb), have also been studied for replacing lead (Pb) in the solar-energy-absorbing materials. Bi- and Sb-based perovskites have better chemical and photochemical stability.[10,11] In this perspective paper, we are interested in reporting types of $A_3B_2X_9$ perovskites. We studied the structure stability and applications of various compounds based on Bi and Sb. In the case of bismuth, a large series of compositions have been reported, including $Cs_3Bi_2I_9$ (X = I, Cl, Br)[12−16] and $MA_3Bi_2I_9$,[10,17,18] and in the case of antimony, stable compounds $MA_3Sb_2I_9$,[19−21] $Cs_3Sb_2I_9$,[11,22,23] and $Rb_3Sb_2I_9$[24] were reported.

2.1. Bismuth (Bi)-Based Trivalent Halide Perovskites.

Bismuth (Bi) is closer to lead (Pb) in the periodic table and shows a similar electronic configuration to Pb. These perovskites can transform into zero-dimensional dimers of face-sharing BX_6 octahedra (space group $P6_3/mmc$) when A-site cations are substituted with large organic molecules such as $CH_3NH_3^+$. Among all of the reported bismuth-based perovskites, organic−inorganic hybrid bismuth halide $MA_3Bi_2I_9$ is the most studied polymorph type. Öz et al. fabricated thin films of zero-dimensional methylammonium iodo bismuthate $(CH_3NH_3)_3Bi_2I_9$ perovskite using a single-step spin-coating approach. It was found that $(CH_3NH_3)_3Bi_2I_9$ has a hexagonal space group $P6_3/mmc$. Owing to the trivalent state of Bi^{3+}, the solid structure of $MA_3Bi_2I_9$ features two face-sharing 0D perovskite structures, which is constructed by the MA^+ surrounding binuclear octahedral $(Bi_2I_9)^{3-}$ clusters, and all of these are interlinked via hydrogen bonding.[10,17] By studying the electronic structure and optical properties, the first

https://doi.org/10.1021/acsomega.1c05333
ACS Omega 2021, 6, 33240−33252

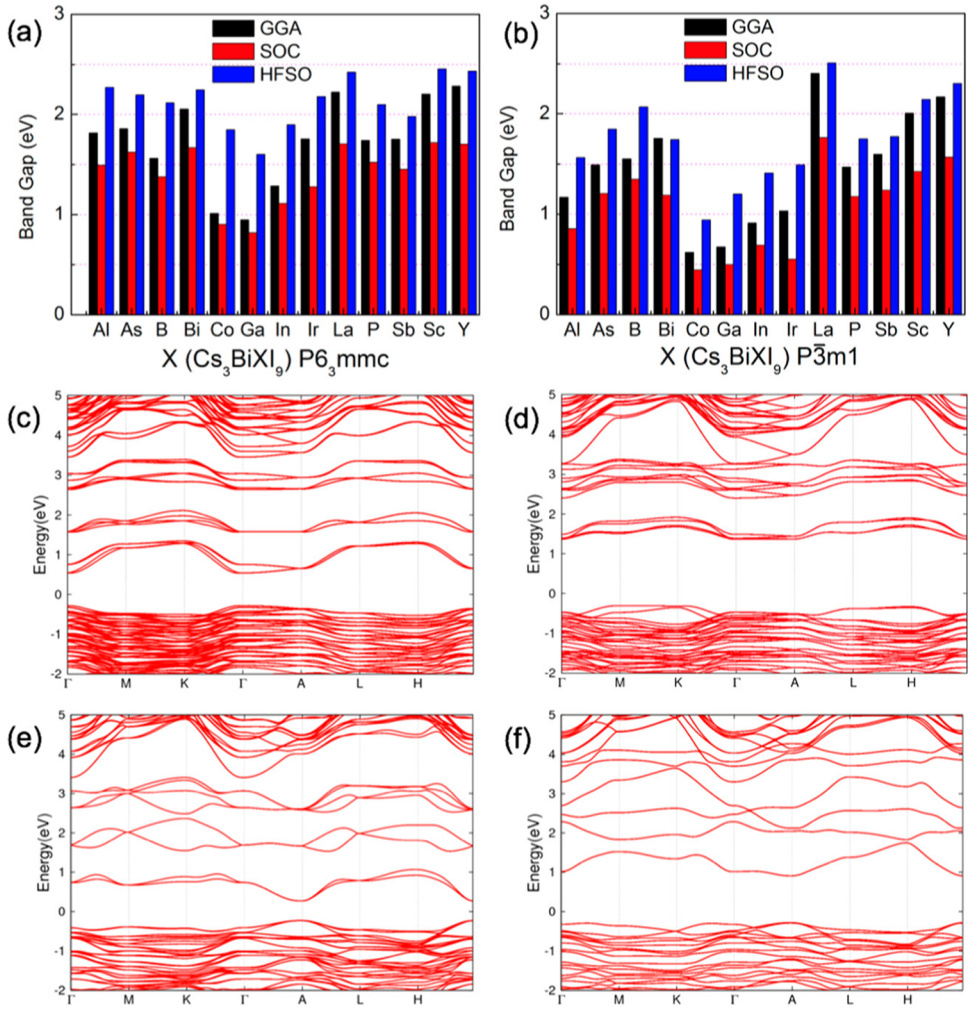

Figure 2. Schematic showing band gaps for (a) the space group $P6_3/mmc$ and (b) the space group $P\bar{3}m1$ of Cs_3BiXI_9 (X = Al, As, B, Bi, Co, Ga, In, Ir, La, P, Sb, Sc, Y). The band structures of (c) Cs_3BiGaI_9 ($P6_3/mmc$), (d) $Cs_3Bi_2I_9$ ($P6_3/mmc$), (e) Cs_3BiGaI_9 ($P\bar{3}m1$), and (f) $Cs_3Bi_2I_9$ ($P\bar{3}m1$). Reprinted with permission from ref 12. Copyright 2017 American Chemical Society.

excitonic peak for the $MA_3Bi_2I_9$ light absorber was observed at 2.45 eV. This was large for photovoltaic applications.[10]

The layered-solution crystal-growth method was used to obtain high-quality single crystals of $MA_3Bi_2I_9$. The BiI_6 octahedra in $MA_3Bi_2I_9$ are linked by face-sharing, while one-third of the octahedral B^{3+} sites are vacant to maintain charge neutrality. At room temperature, $MA_3Bi_2I_9$ has a high dielectric constant. It has been observed that the nature of $MA_3Bi_2I_9$ changed with temperature variation. The antipolar nature observed at 300 K exhibited the hexagonal space group $P6_3/mmc$. At the temperatures of 160 and 143 K, the structure was found to be transformed from the hexagonal space group $P6_3/mmc$ to the monoclinic space groups $C2/c$ and $P2_1$.[25] Kim et al. reported similar lead-free hybrid perovskites like $A_3B_2X_9$ with different compositions (A = Cs, MA, FA, EA; B = As, Sb, Bi; X = Cl, Br, I), where MA is methylammonium, FA is formamidinium, and EA is ethylammonium. The crystal structures of $A_3B_2X_9$ were observed in two types of hexagonal $P6_3/mmc$ (dimer) and trigonal $P\bar{3}m1$ (layer) structures,[11,12] as shown in Figure 1. The materials $Cs_3Bi_2I_9$, $MA_3Bi_2I_9$, and $FA_3Bi_2I_9$ have been reported to be an indirect band gap, and the crystal structure for $EA_3Bi_2I_9$ has not been reported yet. The optical band gap of $MA_3Bi_2I_9$ was reported to be 1.94–2.26 eV. The band gap can be tuned from the A-site and B-site substitution; the B-site substitution was very difficult due to simultaneously being influenced by the electronegativity difference and the B–X–B angle.[11,26] Zhang et al. designed a derivative MP–T–BiI_6 (MP = 4-methylpiperidinium; T = I3) from MP–Bi_2I_9, and they found an improvement in the band gap when using it as a hybrid perovskite. To obtain MP–T–BiI_6, they evaporated a mixture, containing 4-methylpiperidine (0.99 g, 10 mmol) and Bi_2O_3 (1.16 g, 2.5 mmol) in 30 mL of HI (47%) solution at room temperature, and after a few days of reaction, red needle crystals of MP-Bi_2I_9 were obtained. Again, they redissolved them in an oxidized hydroiodic acid solution and after a few days of slow evaporation reaction, brownish bulk crystals were obtained. MP–Bi_2I_9 adopted a zero-dimensional (0D) perovskite-like structure that exhibited the centrosymmetric space group of Pnm, and MP–T–BiI_6 belonged to the triclinic family with a space group of $P\bar{1}$ at 290 K. For this new derivative, the MP–T–BiI_6 band gap was found to be 1.56 eV, which was lesser than the band gap of MP–Bi_2I_9 (1.9 eV).[19] The partial exchange of iodide to chloride ions in the $MA_3Bi_2I_9$ perovskite led to the new halogenobismuthate(III) semiconductor $(CH_3NH_3)_6BiI_{5.22}Cl_{3.78}$, which exhibited a different crystal structure. Experimentally and theoretically, the band gaps were obtained at 2.25 and 2.50 eV.[27]

https://doi.org/10.1021/acsomega.1c05333
ACS Omega 2021, 6, 33240–33252

Apart from the use of $MA_3Bi_2I_9$ perovskite as a light absorber in solar cells, this can be used to fabricate an electrochemical double-layer capacitor and used as a photocatalyst for hydrogen production.[17,18] An $MA_3Bi_2I_9$-based electrochemical double-layer capacitor was fabricated by Pious et al. in 2007. They obtained a maximum areal capacitance of 5.5 mF at a scan rate of 5 mV s^{-1}, and this was assumed to be the highest value for a hybrid perovskite-based capacitor.[17] Guo et al. prepared $MA_3Bi_2I_9$ using a simple hydrothermal route and characterized its photocatalytic activity. For $MA_3Bi_2I_9$, the photocatalytic rate for H_2 production was obtained at 12.19 μmol g^{-1} h^{-1}. When platinum (Pt) was deposited on the surface of $MA_3Bi_2I_9$ as a cocatalyst, the photocatalytic rate increased. The $MA_3Bi_2I_9$/Pt sample, which was prepared with 40 mg of $MA_3Bi_2I_9$ and 2 mg of $H_2PtCl_6{\cdot}6_{H_2}O$, showed an excellent photocatalytic rate (169.21 μmol g^{-1} h^{-1}) for H_2 production 14 times that of $MA_3Bi_2I_9$.[18]

Bismuth-based lead-free hybrid perovskites showed good stability under atmospheric conditions but poor efficiency for photovoltaic applications. The efficiency can be increased by fabricated thin films of $MA_3Bi_2I_9$ perovskite with TiO_2 layers.[28,29] Ahmad et al. have reported a one-dimensional (1D)-polymeric chain-based $[(CH_3NH_3)_3Bi_2Cl_9]n$ perovskite.[28] The 1D layers of $MA_3Bi_2X_9$ (X = Cl, I) can be prepared by single-step spin-coating[30] and the two-step soaking-assisted method.[31,32] To achieve better photovoltaic performances, $MA_3Bi_2I_9$ was fabricated with all three configurations of TiO_2 (planar, mesoporous brookite, and anatase TiO_2).[30,32] The samples of the $MA_3Bi_2I_9$ perovskite prepared on the anatase TiO_2 mesoporous layer showed good film coverage and reduced junction resistance as well as charge recombination, giving values better than those on planar and brookite mesoporous layers.[33]

Moreover, all inorganic bismuth iodide perovskites $A_3Bi_2X_9$ (A = Cs, Rb; X = I, Br) have been reported in refs 13, 34, 35. Further, the main issue with $A_3Bi_2X_9$ was its large band gap, which was relatively large to be used in a single-junction solar cell (1.9−2.2 eV for $Cs_3Bi_2I_9$). It has been demonstrated that Cs-based perovskites are indirect, while Rb-based ones have a direct band gap. A theoretical and experimental study was carried out to reduce the band gap by alloying metal substitution.[12,13] The In (indium)- and Ga (gallium)-doped Bi-based perovskites were obtained through density functional theory (DFT) calculations, band structures, and electronic properties determined using the Vienna ab initio simulation package (VASP). The spin−orbit coupling was used to compare various hybrid perovskites. The $Cs_3Bi_2I_9$ has a hexagonal structure space group $P6_3/mmc/P\bar{3}m1$ similar to $MA_3Bi_2I_9$. The band gap of $Cs_3Bi_2I_9$ was found to be indirect. When the $Cs_3Bi_2I_9$ perovskite was doped with Ga and In, the structure exhibited a direct band gap because the valence band maximum shifted near the Γ-point. When Bi was replaced with Ga, the band gap of the Cs_3BiGaI_9 space group $P6_3/mmc/P\bar{3}m1$ (Figure 2) was obtained as 1.60/1.20 eV, which was lower than that of $Cs_3Bi_2I_9$ by 0.65/0.54 eV, while in the case of Cs_3BiInI_9, the band gap was smaller than that of Cs_3BiGaI_9 by 0.3 eV.[12,14] The valance band was formed due to Ga p and In p having a lower energy than the valence band maximum (VBM), and conduction bands were formed with the hybridization of I sp, Bi p, and In/Ga s orbitals. It has been demonstrated that the $Cs_3Bi_2I_9$ perovskite with a $P\bar{3}m1$ symmetry was more appropriate for realizing a lower band gap.[36] The $A_3Bi_2X_9$ perovskites can be converted into double perovskites. Recently in 2020, Peedikakkandy et al. prepared a three-dimensional (3D) Cs_2NaBiI_6 double perovskite by incorporating an alkali metal sulfide group Na_2S in $Cs_3Bi_2I_9$; the results showed that the band gap reduced, and this was introduced as a new family member of lead-free hybrid perovskites. The ionic radius of Na^+ (102 pm) closely agreed with that of Bi^{3+} (103 pm). In ternary perovskites such as $Cs_3Bi_2I_9$, the valence band has a strong Bi 6s and I 5p antibonding character, whereas the conduction band is predominantly formed through the Bi 6p states. The $Cs_3Bi_2I_9$ perovskite was p-type in nature, while the Cs_2NaBiI_6 double perovskite had an n-type nature.[13] Another Bi-based perovskite $Cs_3Bi_2Br_9$ has been reported in refs 37, 38. The structure of pure $Cs_3Bi_2Br_9$ was found to be crystallized in a $P1(1)$-monoclinic form, and it possesses both direct and indirect band gaps for an optically allowed transition; the direct/indirect band gap of $Cs_3Bi_2Br_9$ was found to be 2.67/2.62 eV. The $Cs_3Bi_2Br_9$ perovskite belongs to the hexagonal phase with space group $P\bar{3}m1$.[37,38] First, DFT was used for structure investigation of the bulk $Cs_3Bi_2Br_9$ perovskite; the valence band was composed of Br 4p orbitals to the conduction band (CB) majorly contributed by Bi 6p orbitals hybridized with a small amount of Br 4p orbitals. Further, the given information was demonstrated by optical transient absorption (OTA) and X-ray transient absorption (XTA) spectroscopies.[34]

The other possibility was carried out for reducing the band gap of Bi-based perovskites by alloying another halide at the Bi^{2+} site.[38] The trivalent cations form $A_3B_2X_9$ structures with 2/3 occupancy of the B sites and 1/3 remaining vacant of the same $A_3B_2X_9$ perovskite formula. Ghosh et al., in 2020, reported a $Cs_3Bi_2Br_{9(1-x)}I_{9x}$ perovskite and observed electronic and optical properties at different ratios of Br to I. The radius of Br^- is lower than that of I^-, resulting in reduced d-spacing. It has been observed that the phase did not change until 40% I^- alloying ($Cs_3BiBr_{5.4}I_{3.6}$). The replacement of terminal Bi−I bonds by Bi−Br bonds in BiI_6 octahedra alloyed $BiI^{6-x}Br^x$ octahedra. For $Cs_3BiBr_{4.5}I_{4.5}$ emission, maxima were observed at 486 nm, and the photocurrent gain value was found to be approximate 12, which is larger than $Cs_3Bi_2Br_9$.[37] The substitution of Pb^+ in layered $Cs_3Bi_2Br_9$ halide perovskites enhanced the visible-light absorption. Recently in 2020, Roy et al. synthesized a Pb-substituted $Cs_3Bi_2Br_9$ bulk perovskite by the chemical reprecipitation method. Pb has a +2 oxidation state, whereas Bi has a +3 oxidation state; thus, when Bi is replaced with Pb, it leads to charge imbalance in the compound, creating new states above the valance band because of Pb s and Br p antibonding orbitals. The crystal structure of $Cs_3Bi_2Br_9$ remained unchanged after Pb substitution because the radius of Pb (1.19 Å) is nearly equal to that of Bi (1.03 Å). It was observed that the size of the Pb-substituted $Cs_3Bi_2Br_9$ perovskite increased from 52 to 115 nm when the Pb concentration increased, while the band gap reduced from 2.62 to 2.23 eV on increasing the Pb concentration.[38]

A new nontoxic Bi-based all-inorganic semiconductor $Rb_4Ag_2BiBr_9$ was reported by Sharma et al. in 2019. This was the first compound discovered in the quaternary Rb−Ag−Bi−Br phase diagram that adopted a new structure (Pearson's code oP32). According to density functional theory (DFT) predictions, this compound provided a nearly direct band gap (slightly indirect) of 1.69 eV. Moreover, $Rb_4Ag_2BiBr_9$ was stable in ambient air for several weeks.[35]

https://doi.org/10.1021/acsomega.1c05333
ACS Omega 2021, 6, 33240−33252

Table 1. Summary of Selected Trivalent and Mixed Double Halide Lead-Free Hybrid Perovskites

B cation	perovskites	space group	E_{gap} (eV)	V_{oc}(V)	PCE (%)	J_{sc} (mA cm^{-2})	refs
trivalent	$(MA)_3Bi_2I_9$	$P6_3/mmc$	1.9−2.2	0.66	0.12	0.52	10, 17, 47
	$Cs_3Bi_2I_9$	$P6_3/mmc$	2.2	0.85	1.09	2.15	47
	$(MA)_3Sb_2I_9$	$P6_3/mmc$	2.0/2.5	0.89	0.5	1	11, 48
	$Cs_3Sb_2I_9$	$P6_3/mmc/P\bar{3}m1$	2.05	0.31	≤0.1		49
	$Cs_3Sb_2Br_9$		2.36				44
	$Rb_3Sb_2I_9$	$P1c1$	2.24	0.55	0.66	2.11	24, 50
	$(C_6H_{14}N)_3Bi_2I_9$		2.02				19
	$EA_3Bi_2I_9$		2.03				11
double halide	$Cs_2AgBiBr_6$	$Fm\bar{3}m$	1.95, 2.19	1.01	2.2	3.19	51−53
	$Cs_2AgBiCl_6$	$Fm\bar{3}m$	2.77, 2.3−2.5				52, 54
	Cs_2AgBiI_6	$Fm\bar{3}m$	1.75				55
	$Cs_2AgSbCl_6$	$Fm\bar{3}m$	2.54				56
	Cs_2NaBiI_6	$P6_3/mmc$	1.66	0.47	0.42	1.99	57, 58
	$Cs_2AgInCl_6$	$Fm\bar{3}m$	3.3				59, 60
	$Cs_2AgFeCl_6$	$Fm\bar{3}m$	1.65				61
	$Cs_2AgSbBr_6$	$Fm\bar{3}m$	1.46	0.35	0.01	0.08	62, 63

2.2. Antimony (Sb)-Based Trivalent Halide Perovskites. Antimony is a trivalent (Sb^{3+}) cation that possesses a similar electronic configuration as divalent Pb^{2+}. Sb is expected to be nontoxic, which exhibits a similar atomic structure and properties to those of Bi. Sb-based perovskites like $MA_3Sb_2I_9$,[20,39] $Cs_3Sb_2I_9$,[40,41] $Rb_3Sb_2I_9$,[24,42] $(C_4H_8NH_2)_3Sb_2Cl_9$,[43] and $Cs_3Sb_2Br_9$[23,44] have been reported. It was found that Sb-based $MA_3Sb_2I_9$ and $Cs_3Sb_2I_9$ perovskites displayed band gaps of 1.92 and 2 eV, respectively. The band gap of pure end-member $MA_3Sb_2I_9$ films was reported to be 2.36 eV.[45] The Sb-based perovskites with the organic cation MA^+ ($MA_3Sb_2I_9$) only formed the 0D hexagonal space group $P6_3/mmc$ (dimer) structure, in which octahedral units $(Sb_2I_9)^{3-}$ are surrounded by the $(MA)^+$ cation, whereas the $Cs_3Sb_2I_9$ perovskite can be formed by both types of dimer (space group $P6_3/mmc$) and layered 2D (space group $P\bar{3}m1$) structures, which depend on the synthesized method.[20,46] Ju et al. in 2018 prepared a Sn-doped $MA_3Sb_2I_9$ perovskite and investigated its optoelectronic properties. The electronic and optical properties were also predicted by DFT calculations. It was observed that when Sn^{2+} is substituted in $MA_3Sb_2I_9$, the band gap reduced from 1.92 to 1.43 eV. The VBMs in $MA_3Sb_2I_9$ and Sn-doped $MA_3Sb_2I_9$ are contributed mostly by Sb 5s and I 5p and to a lesser extent by Sn 5s/I 5p orbitals, whereas the CBM of both crystals is contributed by Sb 5p and I 5p orbitals. Both crystals have good thermal stability.[46] Chatterjee and Pal in 2018 substituted Sn^{4+} in $MA_3Sb_2I_9$ and found a reduction in the band gap by 0.44 eV. When Sb^{3+} was replaced by Sn^{4+}, free electrons were produced and started staying in the middle of energy levels, and because of this, the electronic conductivity of the material changed from p-type to n-type.[20] Again in 2020, Chatterjee et al. substituted Bi in $MA_3Sb_2I_9$ for achieving the narrowest band gap, and it could be reduced from end-member $MA_3Sb_2I_9$ (2.36 eV) to $MA_3Sb_{0.5}Bi_{0.5}I_9$ (1.90 eV).[45] The 2D layers of $MA_3Sb_2I_9$ can be prepared by partial substitution of Sb(III) by Pb(II) in the $MAPbI_3$−$MA_3Sb_2I_9$ interface. It was observed that the substituted Sb does not fully incorporate into the structure but rather acts as a surface layer.[21]

In Table 1, we have provided the chemical formula, space group, E_{gap} (band gap), V_{oc} (open-circuit voltage), PCE (power conversion efficiency), and J_{sc} (short-circuit current density) of nontoxic trivalent and double halide perovskites.

Similarly, Sb-based $Cs_3Sb_2I_9$ and $Rb_3Sb_2I_9$ perovskites have been reported for photovoltaic applications.[22,40] The material $Rb_3Sb_2I_9$ was found in a distorted monoclinic layered structure with space group $P2_1/n$, and the band gap was obtained to be 2.03 eV. In the case of $Cs_3Sb_2I_9$ (1.89 eV), both structures can be formed either dimer or layer. These materials have demonstrated high resistivities, ranging from 1010 to 1012 Ω·cm.[22] Recently in 2020, Pradhan et al. reported a new $Cs_3Sb_2Cl_9$ perovskite. Using the XRD study, the compound $Cs_3Sb_2Cl_9$ was found in two phases: trigonal and orthorhombic; the trigonal phase existed at temperatures below 85 °C, while the orthorhombic phase existed above 130 °C. They observed that at a high temperature (300 °C), the orthorhombic phase completely transformed to the trigonal phase. The phase of $Cs_3Sb_2Cl_9$ can also be transformed by Bi substitution. Experimentally, the indirect band gap for the trigonal/orthorhombic phase was observed to be 2.89/2.86 eV, while theoretically, it was observed to be 2.41/2.39 eV.[64] Moreover, Sb-based perovskites have been used in light-emitting diodes (LEDs). Singh et al. synthesized Sb-based 2D perovskites $Cs_3Sb_2Cl_9$, $Cs_3Sb_2Br_9$, and $Cs_3Sb_2I_9$ using the vapor-anion-exchange method. The materials $Cs_3Sb_2Br_9$ and $Cs_3Sb_2I_9$ showed p-type conductivity, while $Cs_3Sb_2Cl_9$ showed n-type conductivity. They reported the first lead-free perovskite LED based on 2D $Cs_3Sb_2I_9$ as the emitter. The device prepared by the $Cs_3Sb_2I_9$ film as the active layer provided a red emission.[23] A colloidal method was used to fabricate Sb-based 2D lead-free perovskites. 1-Dodecanol is a polar solvent that can be used as a solvent and a capping agent to enhance the size uniformity of perovskites.[39,44] Wojciechowska et al. reported a new 2D lead-free hybrid ferroelectric (pyrrolidinium)$_3[Sb_2Cl_9]$. It was found that $(C_4H_8NH_2)_3[Sb_2Cl_9]$ has a trigonal $R3m$ crystal structure and it is built up of $[Sb_2Cl_9]^{3-}$ infinite layers, composed of corner-sharing $SbCl_6$ octahedra, and pyrrolidinium counterions balance the negative charge of the layers.[43] 2D and 3D materials are more desirable for photovoltaic applications than 0D materials given their lower band gap and smaller exciton banding energy. The optoelectronic properties of perovskites can be changed with tuning by halide and A- and B-site substitution. Correa-Baena et al. in 2018 reported $A_3Sb_2I_9$ perovskites and observed changes in optoelectronic properties by exchanging the A-site substitution. It was observed that $Cs_3Sb_2I_9$ formed a 0D

https://doi.org/10.1021/acsomega.1c05333
ACS Omega 2021, 6, 33240−33252

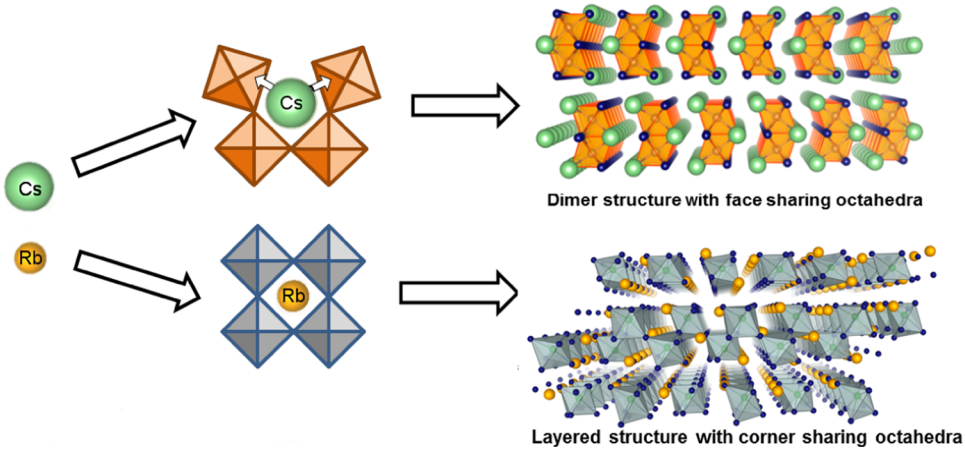

Figure 3. Schematic showing the influence of the A cation size on the structure of $A_3Sb_2I_9$ (A = Cs, Rb). Reprinted with permission from ref 24. Copyright 2016 American Chemical Society.

structure surrounded by SbI_6 octahedra, whereas $Rb_3Sb_2I_9$ formed a 2D layer structure, as shown in Figure 3. The thin films of compounds Cs and K showed indirect band gaps of 2.43 and 2.03 eV, while thin films of Rb showed a direct band gap of 2.02 eV. They also used DFT calculations and obtained band gaps for the Cs, Rb, and K compounds to be 1.89, 1.99, and 2.03 eV, respectively. The highest photocurrent efficiency (0.76%) was observed for $Rb_3Sb_2I_9$.[4242] However, in the dimer phase, the $Cs_3Sb_2I_9$ perovskite has a low charge transport efficiency; various techniques have been developed to transform it into a layered structure. The Rb cations can be accommodated by layered modification (Figure 3). In this paper, the band gap of $Rb_3Sb_2I_9$, which was found to be direct, was 1.98 eV.[24]

Unlike Bi- and Sb-based materials, some new trivalent materials $Rb_3In_2I_9$, $Cs_3In_2I_9$, and $Cs_3Ga_2I_9$ have been reported by Jain et al. The DFT calculations were carried out to analyze crystal structures. They used GGA and HSE06 calculations to predict band structures. The band gaps of $Rb_3In_2I_9$, $Cs_3In_2I_9$, and $Cs_3Ga_2I_9$ materials by HSE06 calculations were obtained to be 2.05, 2.12, and 1.72 eV, respectively. The GGA calculations showed a lower band gap because it is not fully described the many-body effect.[65]

3. LEAD-FREE MIXED DOUBLE HALIDE PEROVSKITES WITH $A_2MM'X_6$ STOICHIOMETRY

Organic−inorganic lead halide perovskites have reached an efficiency of 25.5%.[66] However, toxicity due to the presence of lead, and instability at high temperature and humidity, has impelled researchers to look for more stable and lead-free alternatives, with double halide perovskites being one such family of perovskites. They are of the form $A_2MM'X_6$, where A is a monovalent cation, M is a trivalent metal cation, M′ is a monovalent metal cation, and X is a halide anion.

3.1. Experimental Status of $A_2MM'X_6$ Stoichiometry-Based Mixed Double Halide Perovskites. In 2016, Slavney et al. synthesized crystals of $Cs_2AgBiBr_6$[51] using a concentrated HBr solution that contained CsBr, AgBr, and $BiBr_3$. The space group was $Fm\bar{3}m$ with a red-orange color of the crystal. The lattice parameter was 11.25 Å. The indirect band gap was measured to be 1.95 eV and the direct band gap to be 2.21 eV. In the same year, McClure et al. synthesized Cs_2AgBiX_6 (X = Br, Cl)[52] by both solid-state and solution routes. However, excellent phase purity was observed for samples synthesized via the solution process. The space group was $Fm\bar{3}m$ with lattice parameters 11.2711 Å (X = Br) and 10.7774 Å (X = Cl) and band gaps 2.19 eV (X = Br) and 2.77 eV (X = Cl) measured by diffuse reflectance. Later in 2018, Creutz et al. synthesized colloidal nanocrystals of Cs_2AgBiX_6 (X = Br, Cl)[55] using the hot injection approach. They also synthesized Cs_2AgBiI_6[55] for the first time by anion-exchange reactions. For the complete anion-exchange reaction, TMSX (TMS = trimethylsilyl) reagents were found to be efficient. The XRD pattern of Cs_2AgBiI_6 shows that it has a lattice parameter of 12.09 Å with space group $Fm\bar{3}m$. The band gap observed was 1.75 eV. Another way of synthesizing Cs_2AgBiI_6 nanocrystals is by the antisolvent recrystallization method.[67] In this method, Yang et al. dissolved CsBr, AgBr, and $BiBr_3$ in a dimethyl sulfoxide (DMSO) solvent to form a precursor solution. To precipitate the nanocrystals, isopropanol was used as the antisolvent. Volonakis et al. experimentally synthesized by the solid-state reaction as well as computationally designed $Cs_2AgBiCl_6$[54] using first-principles calculations in the framework of density functional theory (DFT) in local density approximation (LDA). The space group was again found to be $Fm\bar{3}m$. The experimentally and computationally predicted lattice parameters were found to be 10.78 and 10.50 Å, respectively. The optical indirect band gap was found to be in the range of 2.3−2.5 eV estimated from the optical absorption spectrum and the Tauc plot. In 2017, Volonakis et al. also synthesized powdered $Cs_2AgInCl_6$[59] by precipitating $InCl_3$, AgCl, and CsCl in HCl. Unlike the other double perovskites, this system had a direct band gap. Experimentally and computationally, the lattice parameters were found to be 10.47 and 10.20 Å, respectively. The experimentally and computationally predicted direct band gaps were found to be 3.3 eV and (2.7 ± 0.6) eV, respectively. The space group for this system was $Fm\bar{3}m$ as well. Zhou et al. synthesized microcrystals of $Cs_2AgInCl_6$[60] by a hydrothermal method. The lattice parameter was found to be 10.48059 Å. The experimental band gap was reported to be 3.23 eV *via* UV−vis measurement and computationally (using the HSE06 functional) to be 3.33 eV. Tran et al. synthesized polycrystals of both $Cs_2AgInCl_6$ and $Cs_2AgSbCl_6$[56] through solid-state techniques, which involved combining AgCl, CsCl, and $InCl_3(SbCl_3)$ and heating at temperatures of 400 and 210 °C, respectively. Both the structures were cubic having space group $Fm\bar{3}m$ with lattice parameters 10.469 and 10.664 Å, respectively. $Cs_2AgSbCl_6$ was found to be an indirect band-gap

https://doi.org/10.1021/acsomega.1c05333
ACS Omega 2021, 6, 33240−33252

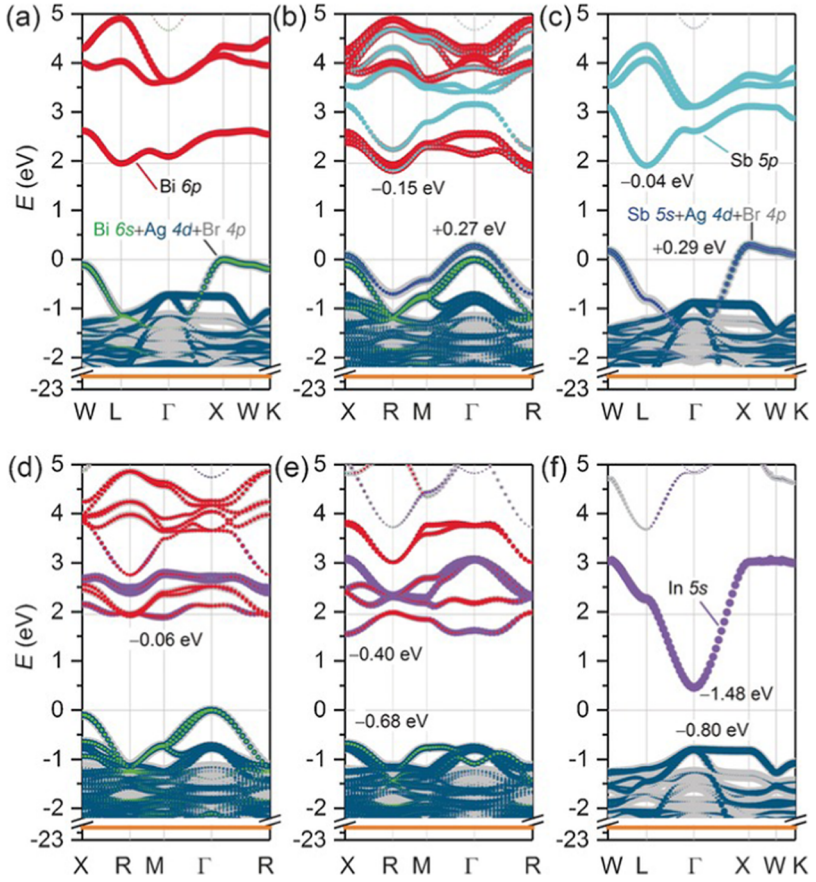

Figure 4. Theoretically (HSE + SOC) calculated band structures of (a) $Cs_2AgBiBr_6$, (b) $Cs_2AgBi_{0.75}Sb_{0.25}Br_6$ (indirect band gap of 1.58 eV), (c) $Cs_2AgSbBr_6$ (the band gap was 1.67 eV), (d) $Cs_2AgBi_{0.75}In_{0.25}Br_6$, (e) $Cs_2AgBi_{0.25}In_{0.75}Br_6$ (the band gap was 2.28 eV), and (f) $Cs_2AgInBr_6$. Reprinted with permission from ref 75. Copyright 2017 Wiley.

semiconductor, whereas $Cs_2AgInCl_6$ had a direct band gap. The UV−vis diffuse reflectance spectra reported the indirect band gap of $Cs_2AgSbCl_6$ to be 2.54 eV and the direct band gap of $Cs_2AgInCl_6$ to be 3.53 eV. The nature of the band gap was validated by DFT-LDA calculations taking into account the spin−orbit coupling (SOC) effect. Another double perovskite system Cs_2NaBiI_6[57] was first reported by Zhang et al. The crystals of Cs_2NaBiI_6 were synthesized using the hydrothermal process at 120 °C for 2 h. After cooling, the crystals were obtained. It was further washed in DI water and centrifuged to obtain the final product. It belongs to the space group $P6_3/mmc$ having a band gap of 1.66 eV. Although Cs_2AgBiX_6 single crystals, polycrystals, and nanocrystals could be synthesized successfully, fabricating good-quality films was inhibited because of the low solubility of precursors. In 2017, Greul et al. successfully synthesized high-quality films of $Cs_2AgBiBr_6$[68] by synthetic routes and also incorporated them in working devices. In this method, CsBr, AgBr, and $BiBr_3$ are dissolved in DMSO to form a precursor solution. The solution along with the substrate is preheated at 75 °C before spin-coating. After spin-coating, the substrate is annealed at 285 °C under ambient conditions for 5 min. This led to the formation of the desired $Cs_2AgBiBr_6$ film. In the same year, Wu et al. synthesized a good-quality film of $Cs_2AgBiBr_6$[69] by low-pressure-assisted solution processing under ambient conditions. In this case, the solution is first spin-coated and then transferred to a low-pressure chamber having 20 Pa pressure. The residual solvent is removed by annealing at 200 °C leading to the formation of a uniform thin film.

3.2. Stability Determination of $A_2MM'X_6$ Stoichiometry-Based Mixed Double Halide Perovskites. One of the major reasons for replacing double halide perovskites with lead-based perovskites is the stability in the former case. The structural stability can be quantitatively determined by Goldschmidt's tolerance factor (t)[70] and octahedral factor (μ). Both of these factors depend on the Shannon ionic radii[71] of A, M, M′, and X. Goldschmidt postulated that perovskites arrange so that "the number of anions surrounding a cation tends to be as large as possible, subject to the condition that all anions touch the cation" (ref 70). This limits the value of t and μ and constitutes the "no-rattling" principle. t and μ can be expressed in the following equations

$$t = \frac{R_A + R_X}{\sqrt{2}(R_{avg} + R_X)} \quad (1)$$

$$\mu = \frac{R_{avg}}{R_X} \quad (2)$$

where $R_{avg} = (R_B + R_{B'})/2$, with R_A and R_X being the Shannon ionic radii of A and X, respectively. For the perovskite to be in the stable structure, t should be between 0.825 and 1.059, whereas μ should be between 0.442 and 0.895.

Recently, Bartel et al. reported a new tolerance factor (τ),[72] which is given by

https://doi.org/10.1021/acsomega.1c05333
ACS Omega 2021, 6, 33240−33252

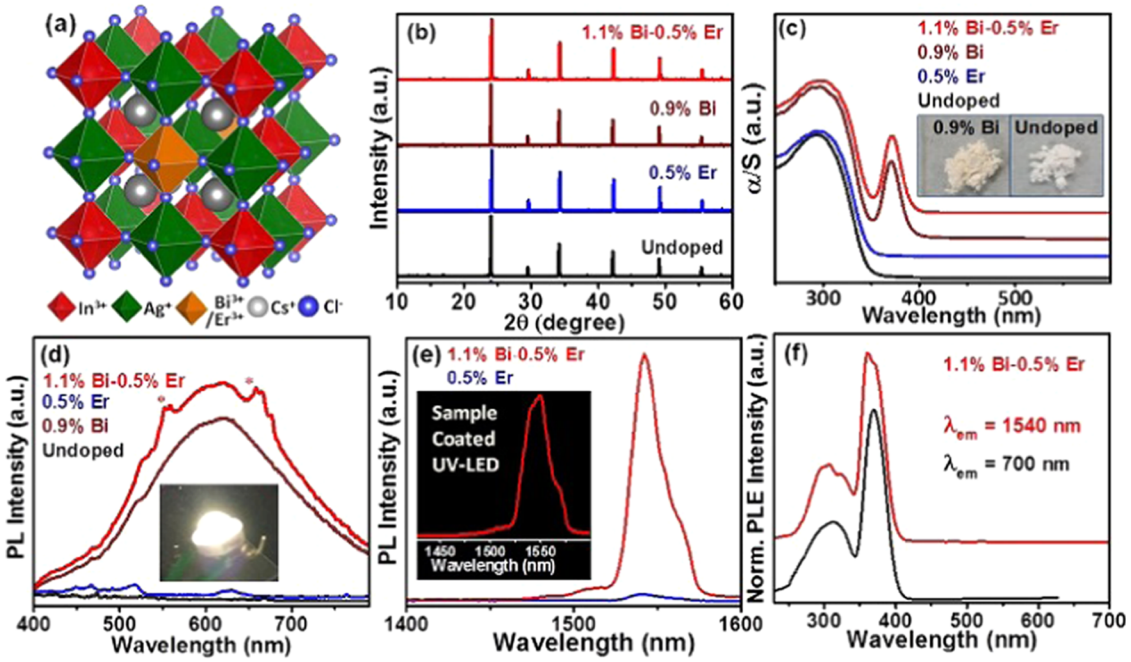

Figure 5. (a) Bi^{3+}−Er^{3+} codoped $Cs_2AgInCl_6$ structure. (b) PXRD of codoped Bi^{3+}−Er^{3+} and Er^{3+}-doped $Cs_2AgInCl_6$. (c) UV−vis absorption spectra of codoped Bi^{3+}−Er^{3+} and Er^{3+}-doped $Cs_2AgInCl_6$. Bi^{3+}-doped and undoped $Cs_2AgInCl_6$ under visible light are shown in insets in (c). (d) Photoluminescence (PL) spectra of pristine $Cs_2AgInCl_6$, Bi^{3+}−Er^{3+} codoped $Cs_2AgInCl_6$, Er^{3+}-doped $Cs_2AgInCl_6$, and Bi-doped $Cs_2AgInCl_6$ in the visible region. Inset of (d) shows a digital photograph of a white-light-emitting diode (LED) from Bi^{3+}−Er^{3+} codoped $Cs_2AgInCl_6$ coated on a commercial UV LED. (e) Near-infrared PL spectra averaged over multiple spots of powder samples mixed with $BaSO_4$ for quantitative comparisons of intensity. Excitation at 370 nm. (f) PL excitation (PLE) spectra of Bi^{3+}−Er^{3+} codoped $Cs_2AgInCl_6$ with emission wavelengths at visible (700 nm) and near-infrared (1540 nm) regions. Reprinted with permission from ref 78. Copyright 2020 Wiley.

$$\tau = \frac{R_X}{R_{avg}} - n_A\left(n_A - \frac{R_A/R_{avg}}{\ln(R_A/R_{avg})}\right) \quad (3)$$

where n_A is the oxidation state of the A-site cation. τ should be less than 4.18 to obtain a stable structure.

(t, μ, τ) for $Cs_2AgBiBr_6$[73] is (0.86, 0.56, 4.21), and for $Cs_2AgBiCl_6$,[73] it is (0.87, 0.60, 4.07). For $Cs_2AgBiBr_{6-x}Cl_x$ mixed halide double perovskites, (t, μ, τ) are in the ranges (0.86−0.87, 0.56−0.60, 4.07−4.21).[73] (t, μ, τ) for $Cs_2AgCrBr_6$, $Rb_2AgCrBr_6$, $K_2AgCrBr_6$, $Cs_2AgCrCl_6$, and Cs_2AgCrI_6 are (0.96, 0.45, 4.04), (0.92, 0.45, 4.14), (0.90, 0.45, 4.22), (0.97, 0.49, 3.87), and (0.94, 0.40, 4.31), respectively.[74]

3.3. Effect of Substitution in $A_2MM'X_6$ Stoichiometry-Based Mixed Double Halide Perovskites. Double halide perovskites are stable and promising candidates for various photovoltaic applications. However, due to their wide and indirect band gaps, they show very low efficiency. This limits their use in varied applications. One of the ways to tune the band gaps is by substitution. In this section, we see how by substituting different elements like Sb, In, Bi, Tl, Mn, and Fe in various double halide perovskites, one can successfully tune the band gaps to optimum value and also modulate the nature of the band gap.

3.3.1. Effect of Sb, In, and Bi Substitution. $Cs_2AgBiBr_6$ is a promising double halide perovskite for photovoltaic applications due to its stability, but its indirect band gap limits its efficiency. Du et al. performed band-gap engineering of $Cs_2AgBiBr_6$[75] by substituting Sb and In in place of Bi. They successfully synthesized $Cs_2AgBi_{1-x}In_xBr_6$ (x = 0, 0.25, 0.50, and 0.75) and $Cs_2AgBi_{1-x}Sb_xBr_6$ (x = 0, 0.125, and 0.375). The In and Sb substituted systems having concentrations greater than x = 0.75 and x = 0.375, respectively, were found to be unstable and hence could not be synthesized. With the increase in concentration of substitution, it was observed that the lattice parameters decreased linearly following Vegard's law.[76] From the Tauc plots, they found that after substituting with Sb and In, the direct band gap varied from 2.15 to 2.41 eV and the indirect band gap varied from 1.86 to 2.27 eV. For In-substituted $Cs_2AgBiBr_6$, the band gap increased from 2.12 to 2.27 eV with an increase in concentration. However, for Sb-substituted $Cs_2AgBiBr_6$, the band gap decreased from 2.12 to 1.86 eV with an increase in concentration. Band structures were also calculated by DFT (HSE06 + SOC) for the substituted systems (Figure 4). From Figure 4b, it can be observed that for $Cs_2AgBi_{0.75}Sb_{0.25}Br_6$, the band gap remains indirect with the value of 1.58 eV. Sb 5s, Ag 4d, and Br 4p orbitals contribute to the valence band. However, Sb 5p orbitals contribute to the conduction band in a similar energy range as Bi 6p orbitals. This resulted in lowering of the CBM by 0.15 eV and elevation of VBM by 0.27 eV, hence decreasing the band gap by Sb substitution, which was in accordance with the experimental results. The band gap for $Cs_2AgSbBr_6$ (Figure 4c) was found to be 1.67 eV. The CBM was lowered by 0.04 eV and the VBM was elevated by 0.29 eV with respect to the CBM and VBM of $Cs_2AgBiBr_6$. The band gap of $Cs_2AgBi_{0.75}In_{0.25}Br_6$ was found to be 0.06 eV less than the band gap of $Cs_2AgBiBr_6$. This contradicted the experimentally perceived band gap where it increased with an increase in the In concentration. This is due to the ordered $BiBr_6$ octahedra in DFT calculation, which is not the case experimentally. For $Cs_2AgBi_{0.25}In_{0.75}Br_6$, the band gap was found to be 2.28 eV, which is in accordance with the experimental trend.

Transition of band gap from indirect to direct was also observed for $Cs_2AgSb_xIn_{1-x}Cl_6$[77] by Tran et al. $Cs_2AgSbCl_6$

https://doi.org/10.1021/acsomega.1c05333
ACS Omega 2021, 6, 33240−33252

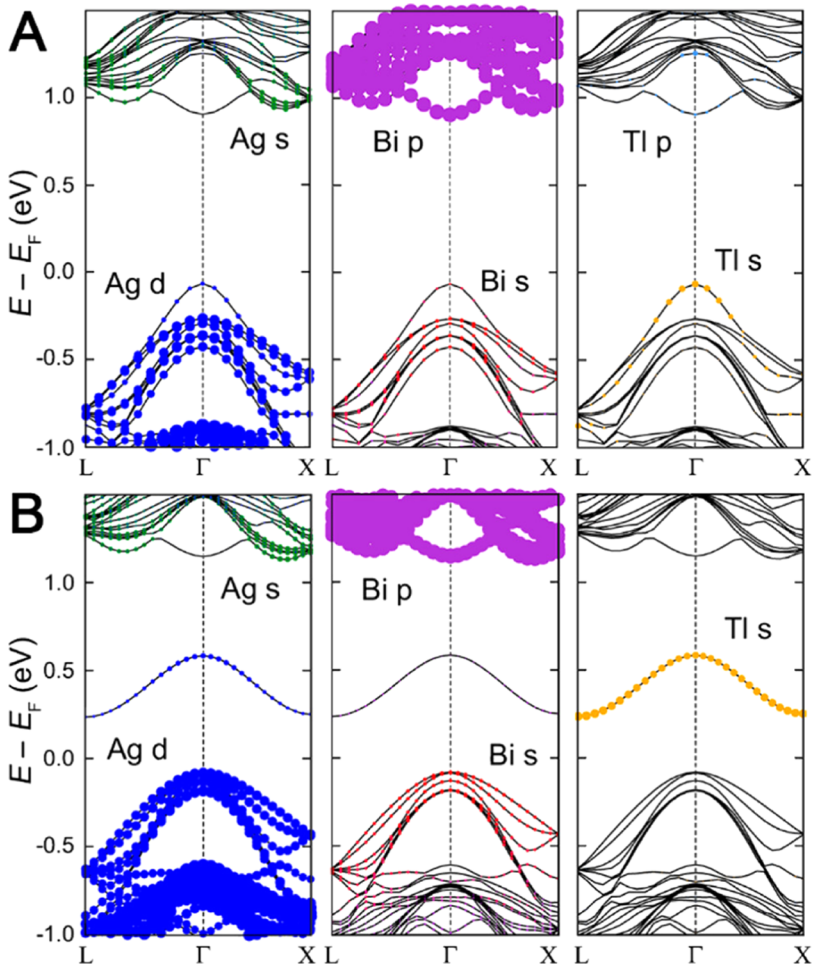

Figure 6. DFT (PBE + SOC)-calculated band structure of $CsAg_{1-a}Bi_{1-b}Tl_xBr_6$ (x = 0.06). (A) Tl substituted at the Ag site (shifting of the nature of band gap from indirect to direct is observed), and (B) Tl substituted at the Bi site (the nature of the band gap remains the same, i.e., indirect). Reprinted with permission from ref 79. Copyright 2017 American Chemical Society.

and $Cs_2AgSb_{0.5}In_{0.5}Cl_6$ have indirect band gaps of 2.54 and 2.81 eV, respectively. For x = 0.4 and 0.2, i.e., $Cs_2AgSb_{0.4}In_{0.6}Cl_6$ and $Cs_2AgSb_{0.2}In_{0.8}Cl_6$, respectively, the band gaps become direct in nature with values of 2.92 and 3.06 eV, respectively. $Cs_2AgInCl_6$ was also observed to have a direct nature of band gap. As the concentration of Sb increased, it was observed that the nature of the band gap altered from direct to indirect with a decrease in the value. The band structures of $Cs_2AgSbCl_6$ and $Cs_2AgInCl_6$ were calculated using local density approximation (LDA) considering spin−orbit coupling (SOC). The SOC effect was more prevalent for $Cs_2AgSbCl_6$ rather than $Cs_2AgInCl_6$ as Sb shows greater relativistic effects than In. Due to the SOC effect, it was observed that the first conduction band of $Cs_2AgSbCl_6$ is split at the energy level of 0.6 eV at the Γ point. From the projected density of states (DOS) of both structures, it was seen that the Ag d and Cl p orbitals contributed to the valence band edge. For $Cs_2AgSbCl_6$, the conduction band is mainly contributed by the Sb 5p orbitals. However, for $Cs_2AgInCl_6$, the conduction band is contributed by In s and Cl p orbitals. As the concentration of Sb increases, the Sb 5s orbital contribution increases in the valence band and the In 5s orbital contribution decreases in the conduction band. This leads to the shift from direct to indirect band gap with the incorporation of Sb.

Codoping of Bi^{3+} with lanthanoids like Er^{3+} and Yb^{3+} in the double halide perovskite $Cs_2AgInCl_6$ shows promising applications in optical fiber communications, near-infrared (NIR) LEDs, and NIR sensors.[78] Ln^{3+} (Ln = Er and Yb)-doped double perovskites by Arfin et al. showed a weak near-infrared emission intensity and a high excitation energy (≤350 nm). However, after codoping it with Bi^{3+}, the projected density of states (PDOS) at the band edges got modified, which was responsible for the new optical absorption peak at a lower energy (372 nm), as shown in Figure 5. This energy that is absorbed gets transferred to the Ln^{3+} f-electrons, promoting the NIR dopant emissions. The PDOS of pristine $Cs_2AgInCl_6$ shows hybridization of Ag 5s, Cs 6s, and Cl 3p orbitals in the conduction band as well as a deeper valence band regime. However, for Bi^{3+}-doped (12.5 atom %) samples, the contribution of Bi at the band edges of both the valence band maximum and the conduction band minimum is significant. This leads to the change in the optical transitions near the band-gap energies.

3.3.2. Effect of Tl, Mn, and Fe Substitution. Band-gap tuning can also be done by substituting Tl[79] in $Cs_2AgBiBr_6$, which leads to a carrier lifetime similar to that of $CH_3NH_3PbI_3$. Slavney et al. substituted Tl^{3+} to tune the band gap of the double perovskite $Cs_2AgBiBr_6$. DFT-calculated energy loss/gain owing to Tl substitution showed that Tl^{3+} substitution at

https://doi.org/10.1021/acsomega.1c05333
ACS Omega 2021, 6, 33240−33252

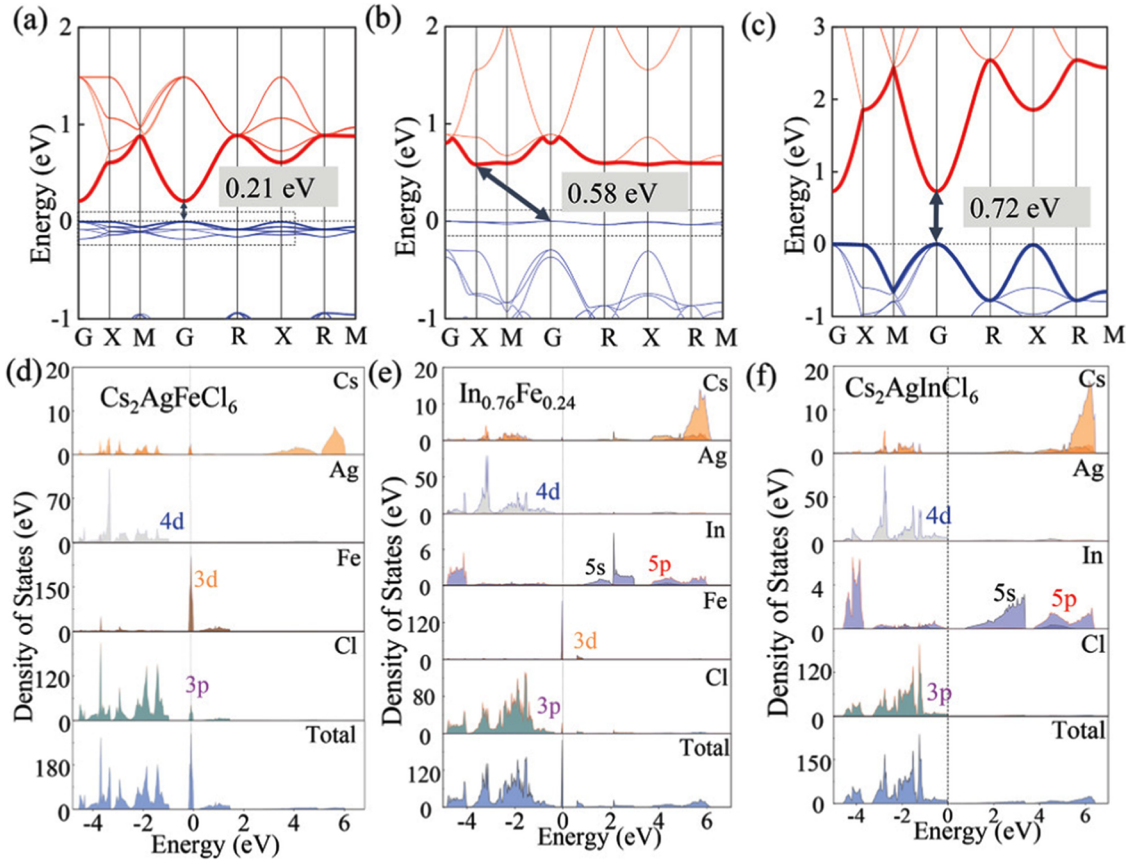

Figure 7. DFT (PBE)-calculated band structures of (a) $Cs_2AgFeCl_6$ (direct band-gap nature), (b) $Cs_2AgIn_{0.76}Fe_{0.24}Cl_6$ (indirect band-gap nature), and (c) $Cs_2AgInCl_6$ (direct band-gap nature). Total and projected density of states (PDOS) of (d) $Cs_2AgFeCl_6$, (e) $Cs_2AgIn_{0.76}Fe_{0.24}Cl_6$, and (f) $Cs_2AgInCl_6$. Reprinted with permission from ref 61. Copyright 2020 Wiley.

the Bi site is not favorable with energy $\Delta E = 0.7$ eV. However, for substitution at the Ag site, the energy was $\Delta E = -0.05$ eV, which is energetically favorable. Band structure calculations were also performed using the PBE + SOC functional for $CsAg_{1-a}Bi_{1-b}Tl_xBr_6$, where $x = a + b$. For $x = 0.06$, the band-gap nature shifted from indirect to direct with substitution at the Ag site, as shown in Figure 6A. In VBM, the Tl s states were found to be above $Cs_2AgBiBr_6$ states, leading to the reduction of the band gap. In CBM, there is hybridization of Tl p states with Br p and Bi p orbitals leading to the direct nature of the band gap. However, substituting at the Bi site does not change the nature of the band gap and it remains indirect, as observed from Figure 6B. Substitution of Tl at both Ag and Bi sites leads to the indirect nature of the band gap with a reduction in the band gap as well. Here, the VBM is made up of Tl s orbitals rather than Tl p orbitals, which leads to the indirect nature of the band gap.

Visible-light emission in direct band gap $Cs_2AgInCl_6$ by Mn^{3+} doping[80] was observed by Nandha and Nag. Upon illumination by UV light, a red color emission was observed from the Mn-doped $Cs_2AgInCl_6$. The energy absorbed by $Cs_2AgInCl_6$ was transferred to the Mn d electrons. The de-excitation of energy from the Mn d electrons resulted in PL with a lifetime of milliseconds. The intensity of PL emission increased with an increase in the concentration of Mn until 1%. With a greater concentration of Mn, the PL intensity decreased due to the possible Mn−Cl−Mn exchange interactions.[81]

Recently, Yin et al. synthesized stable $Cs_2AgFeCl_6$ as well as $Cs_2AgIn_xFe_{1-x}Cl_6$.[61] The absorbance of these crystals is in the range of 450−800 nm. This amplifies the PL quantum yield by 167 times. Fe 3d and In 5s states lead to an increase in the carrier transport ability in these systems. From the band structure (Figure 7) analysis, it was observed that as the concentration of In increased, the band gap also increased. $Cs_2AgFeCl_6$ and $Cs_2AgInCl_6$ showed direct band gaps, but $Cs_2AgIn_{0.76}Fe_{0.24}Cl_6$ showed an indirect band gap. For $Cs_2AgFeCl_6$ and $Cs_2AgIn_{0.76}Fe_{0.24}Cl_6$, Fe 3d and Cl 3p orbitals contribute to the VBM. The interaction of Fe and Cl atoms promotes the bichannel carrier transport. Fe 3d orbitals have a slightly higher energy than In orbitals below the Fermi level. This leads to lowering of the VBM with an increase in the concentration of In in the system, and hence, an increase in the band gap was observed.

4. SUMMARY AND FUTURE OUTLOOK

In this perspective, we have stressed on different aspects of lead-free perovskite materials, their structure, various opto-electronic properties, and photoconversion efficiency. We have discussed briefly different synthesis techniques like the single-step spin-coating approach, layered-solution crystal growth, two-step soaking-assisted method, etc. The space group and the direct or indirect band gap of perovskite materials are major deciding factors. Here, we have also discussed some of the limitations (toxicity, wide band gap, instability, etc.) and their corrective measures.

Toxicity is the major factor limiting the commercialization of Pb-based perovskites. Another divalent metal substitutes of Pb^{2+}, like Sn^{2+}, is highly unstable and easily gets converted into

https://doi.org/10.1021/acsomega.1c05333
ACS Omega 2021, 6, 33240−33252

Sn^{4+}.[82] The quest for a more stable and less-toxic substitute has opened up channels for trivalent and tetravalent metal substitution. $A_3M_2X_9$ and $A_2MM'X_6$ types of lead-free perovskites have been discussed in this perspective. The $A_3M_2X_9$ type can be illustrated through Sb- and Bi-based perovskites. Antimony (Sb)-based perovskite materials having good optoelectronic properties, excellent stability, and less toxicity have a great future ahead in the field of photovoltaic technology. Along with good features, there exist some shortcomings like a wide band gap, uncontrolled crystallization, weak structural features, and water-sensitive nature. They have a large exciton binding energy and a small exciton diffusion length, which are unfavorable. The band gap of Sb-based perovskites ranges from 1.95 to 2.43 eV, which can be tailored accordingly by introducing some less-toxic metal into the perovskite structure. The addition of new antisolvents can control the crystallization process and hence the structural aspects. The introduction of hydrophobic cations to the perovskite structure can be helpful in improving the water sensitivity of Sn-based perovskites.[83]

Mixed halide double perovskites can be broadly divided into two types, $A_2M(I)M'(III)X_6$ and $A_2M(IV)X_6$. $Cs_2AgBiBr_6$, Cs_2NaBiI_6, and Cs_2TiBr_6 are perovskites used efficiently in photovoltaics.[84] Ag−Bi material-based perovskites have a large indirect band gap that limits their photovoltaic performances. Band-gap engineering including alloying or doping can be performed for reducing the optical band gap; e.g., the band gap of Cs_2TiBr_6 can be tailored by substituting different materials, for decreasing the band gap, Cu, Sb, and Tl can be doped and for increasing the band gap, In can be used as a dopant. $FA_4GeSbCl_{12}$ is a newly discovered double perovskite having a band gap of 1.3 eV.[85] Coming out of the stereotypes, different perovskite features can be optimized through compositional engineering. The domain of double perovskites is very challenging and full of possibilities. Most of the aspects are still untouched and need to be explored in depth to drive the research era toward a new horizon.

AUTHOR INFORMATION

Corresponding Authors

Rajeev Ahuja − *Department of Physics, Indian Institute of Technology Ropar, Rupnagar, Punjab 140001, India; Condensed Matter Theory Group, Department of Physics and Astronomy, Uppsala University, Uppsala 75120, Sweden;* orcid.org/0000-0003-1231-9994; Email: rajeev.ahuja@physics.uu.se, rajeev.ahuja@iitrpr.ac.in

Sudip Chakraborty − *Materials Theory for Energy Scavenging (MATES) Lab, Harish-Chandra Research Institute (HRI) Allahabad, HBNI, Prayagraj (Allahabad) 211 019, India;* orcid.org/0000-0002-6765-2084; Email: sudipchakraborty@hri.res.in, sudiphys@gmail.com

Authors

Dhirendra Kumar − *Materials Theory for Energy Scavenging (MATES) Lab, Harish-Chandra Research Institute (HRI) Allahabad, HBNI, Prayagraj (Allahabad) 211 019, India*

Jagjit Kaur − *Materials Theory for Energy Scavenging (MATES) Lab, Harish-Chandra Research Institute (HRI) Allahabad, HBNI, Prayagraj (Allahabad) 211 019, India*

Prajna Parimita Mohanty − *Department of Physics, Indian Institute of Technology Ropar, Rupnagar, Punjab 140001, India*

Complete contact information is available at: https://pubs.acs.org/10.1021/acsomega.1c05333

Author Contributions

[⊥]Dhirendra Kumar and Jagjit Kaur contributed equally.

Notes

The authors declare no competing financial interest.

ACKNOWLEDGMENTS

The authors would like to acknowledge HRI and IIT Ropar for the infrastructure. The DST-SERB funding SRG/2020/001707 is also acknowledged. R.A. also thanks the Swedish Research Council (VR-2016-06014 and VR-2020-04410) for financial support.

REFERENCES

(1) Wu, W.-Q.; Chen, D.; Caruso, R. A.; Cheng, Y.-B. Recent progress in hybrid perovskite solar cells based on n-type materials. *J. Mater. Chem. A* **2017**, *5*, 10092−10109.

(2) Adjogri, S. J.; Meyer, E. L. A Review on Lead-Free Hybrid Halide Perovskites as Light Absorbers for Photovoltaic Applications Based on Their Structural, Optical, and Morphological Properties. *Molecules* **2020**, *25*, No. 5039.

(3) Frohna, K.; Stranks, S. D. *7 - Hybrid Perovskites for Device Applications*; Woodhead Publishing, 2019; pp 211−256.

(4) Chen, Y.; Zhang, L.; Zhang, Y.; Gao, H.; Yan, H. Large-area perovskite solar cells − a review of recent progress and issues. *RSC Adv.* **2018**, *8*, 10489−10508.

(5) De Oliveira, A. E. R. T. P.; Alves, A. K. *Organic−Inorganic Hybrid Perovskites for Solar Cells Applications*; Springer, 2019; pp 89−101.

(6) Sani, F.; Shafie, S.; Lim, H. N.; Musa, A. O. Advancement on Lead-Free Organic-Inorganic Halide Perovskite Solar Cells: A Review. *Materials* **2018**, *11*, No. 1008.

(7) Roy, P.; Kumar Sinha, N.; Tiwari, S.; Khare, A. A review on perovskite solar cells: Evolution of architecture, fabrication techniques, commercialization issues and status. *Sol. Energy* **2020**, *198*, 665−688.

(8) Chakraborty, S.; Xie, W.; Mathews, N.; Sherburne, M.; Ahuja, R.; Asta, M.; Mhaisalkar, S. G. Rational Design: A High-Throughput Computational Screening and Experimental Validation Methodology for Lead-Free and Emergent Hybrid Perovskites. *ACS Energy Lett.* **2017**, *2*, 837−845.

(9) Sun, S.; et al. Accelerated Development of Perovskite-Inspired Materials via High-Throughput Synthesis and Machine-Learning Diagnosis. *Joule* **2019**, *3*, 1437−1451.

(10) Öz, S.; Hebig, J.-C.; Jung, E.; Singh, T.; Lepcha, A.; Olthof, S.; Jan, F.; Gao, Y.; German, R.; van Loosdrecht, P. H.; Meerholz, K.; Kirchartz, T.; Mathur, S. Zero-dimensional (CH3NH3)3Bi2I9 perovskite for optoelectronic applications. *Sol. Energy Mater. Sol. Cells* **2016**, *158*, 195−201. Nanotechnology for Next Generation High Efficiency Photovoltaics: NEXTGEN NANOPV Spring International School Workshop.

(11) Kim, S.-Y.; Yun, Y.; Shin, S.; Lee, J. H.; Heo, Y.-W.; Lee, S. Wide range tuning of band gap energy of A3B2X9 perovskite-like halides. *Scr. Mater.* **2019**, *166*, 107−111.

(12) Hong, K.-H.; Kim, J.; Debbichi, L.; Kim, H.; Im, S. H. Band Gap Engineering of Cs3Bi2I9 Perovskites with Trivalent Atoms Using a Dual Metal Cation. *J. Phys. Chem. C* **2017**, *121*, 969−974.

(13) Peedikakkandy, L.; Chatterjee, S.; Pal, A. J. Bandgap Engineering and Efficient Conversion of a Ternary Perovskite (Cs3Bi2I9) to a Double Perovskite (Cs2NaBiI6) with the Aid of Alkali Metal Sulfide. *J. Phys. Chem. C* **2020**, *124*, 10878−10886.

(14) Bai, F.; Hu, Y.; Hu, Y.; Qiu, T.; Miao, X.; Zhang, S. Lead-free, air-stable ultrathin Cs3Bi2I9 perovskite nanosheets for solar cells. *Sol. Energy Mater. Sol. Cells* **2018**, *184*, 15−21.

(15) Gu, J.; Yan, G.; Lian, Y.; Mu, Q.; Jin, H.; Zhang, Z.; Deng, Z.; Peng, Y. Bandgap engineering of a lead-free defect perovskite

Cs3Bi2I9 through trivalent doping of Ru3+. *RSC Adv.* **2018**, *8*, 25802−25807.
(16) Ghosh, B.; Chakraborty, S.; Wei, H.; Guet, C.; Li, S.; Mhaisalkar, S.; Mathews, N. Poor Photovoltaic Performance of Cs3Bi2I9: An Insight through First-Principles Calculations. *J. Phys. Chem. C* **2017**, *121*, 17062−17067.
(17) Pious, J. K.; Lekshmi, M. L.; Muthu, C.; Rakhi, R. B.; Nair, V. C. Zero-Dimensional Methylammonium Bismuth Iodide-Based Lead-Free Perovskite Capacitor. *ACS Omega* **2017**, *2*, 5798−5802.
(18) Guo, Y.; Liu, G.; Li, Z.; Lou, Y.; Chen, J.; Zhao, Y. Stable Lead-Free (CH3NH3)3Bi2I9 Perovskite for Photocatalytic Hydrogen Generation. *ACS Sustainable Chem. Eng.* **2019**, *7*, 15080−15085.
(19) Zhang, W.; Liu, X.; Li, L.; Sun, Z.; Han, S.; Wu, Z.; Luo, J. Triiodide-Induced Band-Edge Reconstruction of a Lead-Free Perovskite-Derivative Hybrid for Strong Light Absorption. *Chem. Mater.* **2018**, *30*, 4081−4088.
(20) Chatterjee, S.; Pal, A. J. Tin(IV) Substitution in (CH3NH3)-3Sb2I9: Toward Low-Band-Gap Defect-Ordered Hybrid Perovskite Solar Cells. *ACS Appl. Mater. Interfaces* **2018**, *10*, 35194−35205.
(21) Zhu, F.; Gentry, N. E.; Men, L.; White, M. A.; Vela, J. Aliovalent Doping of Lead Halide Perovskites: Exploring the CH3NH3PbI3−(CH3NH3)3Sb2I9 Nanocrystalline Phase Space. *J. Phys. Chem. C* **2018**, *122*, 14082−14090.
(22) McCall, K. M.; Stoumpos, C. C.; Kostina, S. S.; Kanatzidis, M. G.; Wessels, B. W. Strong Electron−Phonon Coupling and Self-Trapped Excitons in the Defect Halide Perovskites A3M2I9 (A = Cs, Rb; M = Bi, Sb). *Chem. Mater.* **2017**, *29*, 4129−4145.
(23) Singh, A.; Chiu, N.-C.; Boopathi, K. M.; Lu, Y.-J.; Mohapatra, A.; Li, G.; Chen, Y.-F.; Guo, T.-F.; Chu, C.-W. Lead-Free Antimony-Based Light-Emitting Diodes through the Vapor−Anion-Exchange Method. *ACS Appl. Mater. Interfaces* **2019**, *11*, 35088−35094.
(24) Harikesh, P. C.; Mulmudi, H. K.; Ghosh, B.; Goh, T. W.; Teng, Y. T.; Thirumal, K.; Lockrey, M.; Weber, K.; Koh, T. M.; Li, S.; Mhaisalkar, S.; Mathews, N. Rb as an Alternative Cation for Templating Inorganic Lead-Free Perovskites for Solution Processed Photovoltaics. *Chem. Mater.* **2016**, *28*, 7496−7504.
(25) Kamminga, M. E.; Stroppa, A.; Picozzi, S.; Chislov, M.; Zvereva, I. A.; Baas, J.; Meetsma, A.; Blake, G. R.; Palstra, T. T. M. Polar Nature of (CH3NH3)3Bi2I9 Perovskite-Like Hybrids. *Inorg. Chem.* **2017**, *56*, 33−41.
(26) Li, M.-Q.; Hu, Y.-Q.; Bi, L.-Y.; Zhang, H.-L.; Wang, Y.; Zheng, Y.-Z. Structure Tunable Organic−Inorganic Bismuth Halides for an Enhanced Two-Dimensional Lead-Free Light-Harvesting Material. *Chem. Mater.* **2017**, *29*, 5463−5467.
(27) Hoefler, S. F.; Rath, T.; Fischer, R.; Latal, C.; Hippler, D.; Koliogiorgos, A.; Galanakis, I.; Bruno, A.; Fian, A.; Dimopoulos, T.; Trimmel, G. A Zero-Dimensional Mixed-Anion Hybrid Halogenobismuthate(III) Semiconductor: Structural, Optical, and Photovoltaic Properties. *Inorg. Chem.* **2018**, *57*, 10576−10586.
(28) Ahmad, K.; Ansari, S. N.; Natarajan, K.; Mobin, S. M. Design and Synthesis of 1D-Polymeric Chain Based [(CH3NH3)3Bi2Cl9]n Perovskite: A New Light Absorber Material for Lead Free Perovskite Solar Cells. *ACS Appl. Energy Mater.* **2018**, *1*, 2405−2409.
(29) Singh, T.; Kulkarni, A.; Ikegami, M.; Miyasaka, T. Effect of Electron Transporting Layer on Bismuth-Based Lead-Free Perovskite (CH3NH3)3 Bi2I9 for Photovoltaic Applications. *ACS Appl. Mater. Interfaces* **2016**, *8*, 14542−14547.
(30) Zhang, X.; Wu, G.; Gu, Z.; Guo, B.; Liu, W.; Yang, S.; Ye, T.; Chen, C.; Tu, W.; Chen, H. Active-layer evolution and efficiency improvement of (CH3NH33Bi2I9-based solar cell on TiO2-deposited ITO substrate. *Nano Res.* **2016**, *9*, 2921−2930.
(31) Kong, M.; Hu, H.; Wan, L.; Chen, M.; Gan, Y.; Wang, J.; Chen, F.; Dong, B.; Eder, D.; Wang, S. Nontoxic (CH3NH3)3Bi2I9 perovskite solar cells free of hole conductors with an alternative architectural design and a solution-processable approach. *RSC Adv.* **2017**, *7*, 35549−35557.
(32) Jain, S. M.; Phuyal, D.; Davies, M. L.; Li, M.; Philippe, B.; De Castro, C.; Qiu, Z.; Kim, J.; Watson, T.; Tsoi, W. C.; Karis, O.; Rensmo, H.; Boschloo, G.; Edvinsson, T.; Durrant, J. R. An effective approach of vapour assisted morphological tailoring for reducing metal defect sites in lead-free, (CH3NH3)3Bi2I9 bismuth-based perovskite solar cells for improved performance and long-term stability. *Nano Energy* **2018**, *49*, 614−624.
(33) Scholz, M.; Flender, O.; Oum, K.; Lenzer, T. Pronounced Exciton Dynamics in the Vacancy-Ordered Bismuth Halide Perovskite (CH3NH3)3Bi2I9 Observed by Ultrafast UV−vis−NIR Transient Absorption Spectroscopy. *J. Phys. Chem. C* **2017**, *121*, 12110−12116.
(34) Liu, C.; Wang, Y.; Geng, H.; Zhu, T.; Ertekin, E.; Gosztola, D.; Yang, S.; Huang, J.; Yang, B.; Han, K.; Canton, S. E.; Kong, Q.; Zheng, K.; Zhang, X. Asynchronous Photoexcited Electronic and Structural Relaxation in Lead-Free Perovskites. *J. Am. Chem. Soc.* **2019**, *141*, 13074−13080.
(35) Sharma, M.; Yangui, A.; Whiteside, V. R.; Sellers, I. R.; Han, D.; Chen, S.; Du, M.-H.; Saparov, B. Rb4Ag2BiBr9: A Lead-Free Visible Light Absorbing Halide Semiconductor with Improved Stability. *Inorg. Chem.* **2019**, *58*, 4446−4455.
(36) McCall, K. M.; Stoumpos, C. C.; Kontsevoi, O. Y.; Alexander, G. C. B.; Wessels, B. W.; Kanatzidis, M. G. From 0D Cs3Bi2I9 to 2D Cs3Bi2I6Cl3: Dimensional Expansion Induces a Direct Band Gap but Enhances Electron−Phonon Coupling. *Chem. Mater.* **2019**, *31*, 2644−2650.
(37) Ghosh, S.; Mukhopadhyay, S.; Paul, S.; Pradhan, B.; De, S. K. Control Synthesis and Alloying of Ambient Stable Pb-Free Cs3Bi2Br9(1−x)I9x (0 x 1) Perovskite Nanocrystals for Photodetector Application. *ACS Appl. Nano Mater.* **2020**, *3*, 11107−11117.
(38) Roy, M.; Ghorui, S.; Bhawna; Kangsabanik, J.; Yadav, R.; Alam, A.; Aslam, M. Enhanced Visible Light Absorption in Layered Cs3Bi2Br9 Halide Perovskites: Heterovalent Pb2+ Substitution-Induced Defect Band Formation. *J. Phys. Chem. C* **2020**, *124*, 19484−19491.
(39) Yao, M.-M.; Jiang, C.-H.; Yao, J.-S.; Wang, K.-H.; Chen, C.; Yin, Y.-C.; Zhu, B.-S.; Chen, T.; Yao, H.-B. General Synthesis of Lead-Free Metal Halide Perovskite Colloidal Nanocrystals in 1-Dodecanol. *Inorg. Chem.* **2019**, *58*, 11807−11818.
(40) Singh, A.; Boopathi, K. M.; Mohapatra, A.; Chen, Y. F.; Li, G.; Chu, C. W. Photovoltaic Performance of Vapor-Assisted Solution-Processed Layer Polymorph of Cs3Sb2I9. *ACS Appl. Mater. Interfaces* **2018**, *10*, 2566−2573.
(41) Saparov, B.; Hong, F.; Sun, J.-P.; Duan, H.-S.; Meng, W.; Cameron, S.; Hill, I. G.; Yan, Y.; Mitzi, D. B. Thin-Film Preparation and Characterization of Cs3Sb2I9: A Lead-Free Layered Perovskite Semiconductor. *Chem. Mater.* **2015**, *27*, 5622−5632.
(42) Correa-Baena, J.-P.; Nienhaus, L.; Kurchin, R. C.; Shin, S. S.; Wieghold, S.; Putri Hartono, N. T.; Layurova, M.; Klein, N. D.; Poindexter, J. R.; Polizzotti, A.; Sun, S.; Bawendi, M. G.; Buonassisi, T. A-Site Cation in Inorganic A3Sb2I9 Perovskite Influences Structural Dimensionality, Exciton Binding Energy, and Solar Cell Performance. *Chem. Mater.* **2018**, *30*, 3734−3742.
(43) Wojciechowska, M.; Gagor, A.; Piecha-Bisiorek, A.; Jakubas, R.; Ciżman, A.; Zareba, J. K.; Nyk, M.; Zieliński, P.; Medycki, W.; Bil, A. Ferroelectricity and Ferroelasticity in Organic Inorganic Hybrid (Pyrrolidinium)3[Sb2Cl9]. *Chem. Mater.* **2018**, *30*, 4597−4608.
(44) Zhang, J.; Yang, Y.; Deng, H.; Farooq, U.; Yang, X.; Khan, J.; Tang, J.; Song, H. High Quantum Yield Blue Emission from Lead-Free Inorganic Antimony Halide Perovskite Colloidal Quantum Dots. *ACS Nano* **2017**, *11*, 9294−9302.
(45) Chatterjee, S.; Payne, J.; Irvine, J. T. S.; Pal, A. J. Bandgap bowing in a zero-dimensional hybrid halide perovskite derivative: spin−orbit coupling versus lattice strain. *J. Mater. Chem. A* **2020**, *8*, 4416−4427.
(46) Ju, D.; Jiang, X.; Xiao, H.; Chen, X.; Hu, X.; Tao, X. Narrow band gap and high mobility of lead-free perovskite single crystal Sn-doped MA3Sb2I9. *J. Mater. Chem. A* **2018**, *6*, 20753−20759.
(47) Park, B.-W.; Philippe, B.; Zhang, X.; Rensmo, H.; Boschloo, G.; Johansson, E. M. J. Bismuth Based Hybrid Perovskites A3Bi2I9 (A: Methylammonium or Cesium) for Solar Cell Application. *Adv. Mater.* **2015**, *27*, 6806−6813.

https://doi.org/10.1021/acsomega.1c05333
ACS Omega 2021, 6, 33240−33252

(48) Hebig, J.-C.; Kühn, I.; Flohre, J.; Kirchartz, T. Optoelectronic Properties of (CH3NH3)3Sb2I9 Thin Films for Photovoltaic Applications. *ACS Energy Lett.* **2016**, *1*, 309−314.
(49) Saparov, B.; Sun, J.-P.; Meng, W.; Xiao, Z.; Duan, H.-S.; Gunawan, O.; Shin, D.; Hill, I. G.; Yan, Y.; Mitzi, D. B. Thin-Film Deposition and Characterization of a Sn-Deficient Perovskite Derivative Cs2SnI6. *Chem. Mater.* **2016**, *28*, 2315−2322.
(50) Harikesh, P. C.; Mulmudi, H. K.; Ghosh, B.; Goh, T. W.; Teng, Y. T.; Thirumal, K.; Lockrey, M.; Weber, K.; Koh, T. M.; Li, S.; Mhaisalkar, S.; Mathews, N. Rb as an Alternative Cation for Templating Inorganic Lead-Free Perovskites for Solution Processed Photovoltaics. *Chem. Mater.* **2016**, *28*, 7496−7504.
(51) Slavney, A. H.; Hu, T.; Lindenberg, A. M.; Karunadasa, H. I. A Bismuth-Halide Double Perovskite with Long Carrier Recombination Lifetime for Photovoltaic Applications. *J. Am. Chem. Soc.* **2016**, *138*, 2138−2141.
(52) McClure, E. T.; Ball, M. R.; Windl, W.; Woodward, P. M. Cs2AgBiX6 (X = Br, Cl): New Visible Light Absorbing, Lead-Free Halide Perovskite Semiconductors. *Chem. Mater.* **2016**, *28*, 1348−1354.
(53) Gao, W.; Ran, C.; Xi, J.; Jiao, B.; Zhang, W.; Wu, M.; Hou, X.; Wu, Z. High-Quality Cs2AgBiBr6 Double Perovskite Film for Lead-Free Inverted Planar Heterojunction Solar Cells with 2.2 % Efficiency. *ChemPhysChem* **2018**, *19*, 1696−1700.
(54) Volonakis, G.; Filip, M. R.; Haghighirad, A. A.; Sakai, N.; Wenger, B.; Snaith, H. J.; Giustino, F. Lead-Free Halide Double Perovskites via Heterovalent Substitution of Noble Metals. *J. Phys. Chem. Lett.* **2016**, *7*, 1254−1259.
(55) Creutz, S. E.; Crites, E. N.; De Siena, M. C.; Gamelin, D. R. Colloidal Nanocrystals of Lead-Free Double-Perovskite (Elpasolite) Semiconductors: Synthesis and Anion Exchange To Access New Materials. *Nano Lett.* **2018**, *18*, 1118−1123.
(56) Tran, T. T.; Panella, J. R.; Chamorro, J. R.; Morey, J. R.; McQueen, T. M. Designing indirect−direct bandgap transitions in double perovskites. *Mater. Horiz.* **2017**, *4*, 688−693.
(57) Zhang, C.; Gao, L.; Teo, S.; Guo, Z.; Xu, Z.; Zhao, S.; Ma, T. Design of a novel and highly stable lead-free Cs2NaBiI6 double perovskite for photovoltaic application. *Sustainable Energy Fuels* **2018**, *2*, 2419−2428.
(58) Karmakar, A.; Dodd, M. S.; Agnihotri, S.; Ravera, E.; Michaelis, V. K. Cu(II)-Doped Cs2SbAgCl6 Double Perovskite: A Lead-Free, Low-Bandgap Material. *Chem. Mater.* **2018**, *30*, 8280−8290.
(59) Volonakis, G.; Haghighirad, A. A.; Milot, R. L.; Sio, W. H.; Filip, M. R.; Wenger, B.; Johnston, M. B.; Herz, L. M.; Snaith, H. J.; Giustino, F. Cs2InAgCl6: A New Lead-Free Halide Double Perovskite with Direct Band Gap. *J. Phys. Chem. Lett.* **2017**, *8*, 772−778.
(60) Zhou, J.; Xia, Z.; Molokeev, M. S.; Zhang, X.; Peng, D.; Liu, Q. Composition design, optical gap and stability investigations of lead-free halide double perovskite Cs2AgInCl6. *J. Mater. Chem. A* **2017**, *5*, 15031−15037.
(61) Yin, H.; Xian, Y.; Zhang, Y.; Chen, W.; Wen, X.; Rahman, N. U.; Long, Y.; Jia, B.; Fan, J.; Li, W. An Emerging Lead-Free Double-Perovskite Cs2AgFeCl6:In Single Crystal. *Adv. Funct. Mater.* **2020**, *30*, No. 2002225.
(62) Dahl, J. C.; Osowiecki, W. T.; Cai, Y.; Swabeck, J. K.; Bekenstein, Y.; Asta, M.; Chan, E. M.; Alivisatos, A. P. Probing the Stability and Band Gaps of Cs2AgInCl6 and Cs2AgSbCl6 Lead-Free Double Perovskite Nanocrystals. *Chem. Mater.* **2019**, *31*, 3134−3143.
(63) Wei, F.; Deng, Z.; Sun, S.; Hartono, N. T. P.; Seng, H. L.; Buonassisi, T.; Bristowe, P. D.; Cheetham, A. K. Enhanced visible light absorption for lead-free double perovskite Cs2AgSbBr6. *Chem. Commun.* **2019**, *55*, 3721−3724.
(64) Pradhan, A.; Sahoo, S. C.; Sahu, A. K.; Samal, S. L. Effect of Bi Substitution on Cs3Sb2Cl9: Structural Phase Transition and Band Gap Engineering. *Cryst. Growth Des.* **2020**, *20*, 3386−3395.
(65) Jain, A.; Voznyy, O.; Sargent, E. H. High-Throughput Screening of Lead-Free Perovskite-like Materials for Optoelectronic Applications. *J. Phys. Chem. C* **2017**, *121*, 7183−7187.
(66) NREL. Solar Cell Efficiency Chart—Photovoltaic Research—NREL. https://www.nrel.gov/pv/cell-efficiency.html, 2020.
(67) Yang, B.; Chen, J.; Yang, S.; Hong, F.; Sun, L.; Han, P.; Pullerits, T.; Deng, W.; Han, K. Lead-Free Silver-Bismuth Halide Double Perovskite Nanocrystals. *Angew. Chem., Int. Ed.* **2018**, *57*, 5359−5363.
(68) Greul, E.; Petrus, M.; Binek, A.; Docampo, P.; Bein, T. Highly stable, phase pure Cs2AgBiBr6 double perovskite thin films for optoelectronic applications. *J. Mater. Chem. A* **2017**, *5*, 19972−19981.
(69) Wu, C.; Zhang, Q.; Liu, Y.; Luo, W.; Guo, X.; Huang, Z.; Ting, H.; Sun, W.; Zhong, X.; Wei, S.; Wang, S.; Chen, Z.; Xiao, L. The Dawn of Lead-Free Perovskite Solar Cell: Highly Stable Double Perovskite Cs2AgBiBr6 Film. *Adv. Sci.* **2018**, *5*, No. 1700759.
(70) Goldschmidt, V. M. Die Gesetze der Krystallochemie. *Naturwissenschaften* **1926**, *14*, 477−485.
(71) Shannon, R. D. Revised effective ionic radii and systematic studies of interatomic distances in halides and chalcogenides. *Acta Crystallogr., Sect. A* **1976**, *32*, 751−767.
(72) Bartel, C. J.; Sutton, C.; Goldsmith, B. R.; Ouyang, R.; Musgrave, C. B.; Ghiringhelli, L. M.; Scheffler, M. New tolerance factor to predict the stability of perovskite oxides and halides. *Sci. Adv.* **2019**, *5*, No. eaav0693.
(73) Su, J.; Mou, T.; Wen, J.; Wang, B. First-Principles Study on the Structure, Electronic, and Optical Properties of Cs2AgBiBr6-xClx Mixed-Halide Double Perovskites. *J. Phys. Chem. C* **2020**, *124*, 5371−5377.
(74) Varadwaj, P. R. A2AgCrBr6 (A = K, Rb, Cs) and Cs2AgCrX6(X = Cl, I) Double Perovskites: A Transition-Metal-Based Semiconducting Material Series with Remarkable Optics. *Nanomaterials* **2020**, *10*, No. 973.
(75) Du, K.-z.; Meng, W.; Wang, X.; Yan, Y.; Mitzi, D. B. Bandgap Engineering of Lead-Free Double Perovskite Cs2AgBiBr6 through Trivalent Metal Alloying. *Angew. Chem., Int. Ed.* **2017**, *56*, 8158−8162.
(76) Vegard, L. Die Konstitution der Mischkristalle und die Raumfüllung der Atome. *Z. Phys.* **1921**, *5*, 17−26.
(77) Tran, T. T.; Panella, J. R.; Chamorro, J. R.; Morey, J. R.; McQueen, T. M. Designing indirect−direct bandgap transitions in double perovskites. *Mater. Horiz.* **2017**, *4*, 688−693.
(78) Arfin, H.; Kaur, J.; Sheikh, T.; Chakraborty, S.; Nag, A. Bi3+-Er3+ and Bi3+-Yb3+ Codoped Cs2AgInCl6 Double Perovskite Near-Infrared Emitters. *Angew. Chem., Int. Ed.* **2020**, *59*, 11307−11311.
(79) Slavney, A. H.; Leppert, L.; Bartesaghi, D.; Gold-Parker, A.; Toney, M. F.; Savenije, T. J.; Neaton, J. B.; Karunadasa, H. I. Defect-Induced Band-Edge Reconstruction of a Bismuth-Halide Double Perovskite for Visible-Light Absorption. *J. Am. Chem. Soc.* **2017**, *139*, 5015−5018.
(80) Nandha, K. N.; Nag, A. Synthesis and luminescence of Mn-doped Cs2AgInCl6 double perovskites. *Chem. Commun.* **2018**, *54*, 5205−5208.
(81) Nag, A.; Chakraborty, S.; Sarma, D. D. To Dope Mn2+ in a Semiconducting Nanocrystal. *J. Am. Chem. Soc.* **2008**, *130*, 10605−10611.
(82) Baranwal, A. K.; Masutani, H.; Sugita, H.; et al. Lead-free perovskite solar cells using Sb and Bi-based A3B2X9 and A3BX6 crystals with normal and inverse cell structures. *Nano Convergence* **2017**, *4*, No. 26.
(83) Ahmad, K.; Mobin, S. M. Recent Progress and Challenges in A3Sb2X9-Based Perovskite Solar Cells. *ACS Omega* **2020**, *5*, 28404−28412.
(84) Nie, R.; Sumukam, R. R.; Reddy, S. H.; Banavoth, M.; Seok, S. I. Lead-free perovskite solar cells enabled by hetero-valent substitutes. *Energy Environ. Sci.* **2020**, *13*, 2363−2385.
(85) Jin, Z.; Zhang, Z.; Xiu, J.; Song, H.; Gatti, T.; He, Z. A critical review on bismuth and antimony halide based perovskites and their derivatives for photovoltaic applications: recent advances and challenges. *J. Mater. Chem. A* **2020**, *8*, 16166−16188.

https://doi.org/10.1021/acsomega.1c05333
ACS Omega 2021, 6, 33240−33252